Posterior Cramér-Rao Bounds for Doppler Biased Distributed Tracking

XIUFENG SONG
PETER WILLETT
SHENGLI ZHOU

This paper investigates distributed tracking with *range-Doppler coupling*, where a range measurement of a target of interest is linearly biased by its range-rate (or Doppler). The coupling parameter λ can be zero, positive, or negative. The posterior Cramér-Rao bound (PCRB) is derived for distributed radar systems: multistatic and multiple-input multiple-output (MIMO) settings. In the multistatic case, a positive λ leads to the lowest PCRB, the same as is true for monostatic tracking. The paper also compares the tracking performance of multistatic and MIMO configurations, where the latter utilizes two waveforms with $\pm\lambda$ parameters, respectively. Regarding the power-unlimited case, a MIMO radar can always outperform a multistatic one from a tracking perspective. However, if the total power is limited, the situation is somewhat different: the transmitter co-located configuration is worse than a multistatic one, while in the widely-separated case the better choice depends on geometry.

Manuscript received August 31, 2011; revised October 27, 2011; released January 12, 2012.

Refereeing of this contribution was handled by Huimin Chen.

This work was supported by the U.S. Office of Naval Research under Grants N00014-07-10429 and N00014-09-10613.

Authors' address: Department of Electrical and Computer Engineering, University of Connecticut, 371 Fairfield Way Unit 2157, Storrs, CT 06269, E-mail: (xiufeng.song@gmail.com; willett@engr.uconn.edu; shengli@engr.uconn.edu).

1. INTRODUCTION

A radar receiver extracts the range information of a moving target with a matched filter, of which the output is a slice of the waveform ambiguity function (AF) at Doppler shift f_d instead of zero in the absence of noise [6]. As a consequence, mismatch occurs and detection will degrade. To combat performance degradation of matched filtering against unknown Doppler shifts, Doppler tolerant (or insensitive) waveforms (DTWs), such as linear frequency modulation (LFM), P3 and P4 codes [6], appeared via introducing a slowly decaying *ridge* to their AFs as shown in Fig. 1. The range-Doppler ridge enables the matched filter to produce a slightly lower peak amplitude so as to avoid detection failure, but at the expense of introducing range bias [2], [6], [14], [15]. This phenomenon is termed *range-Doppler coupling*, and it is a compromise between range accuracy and Doppler robust detection.

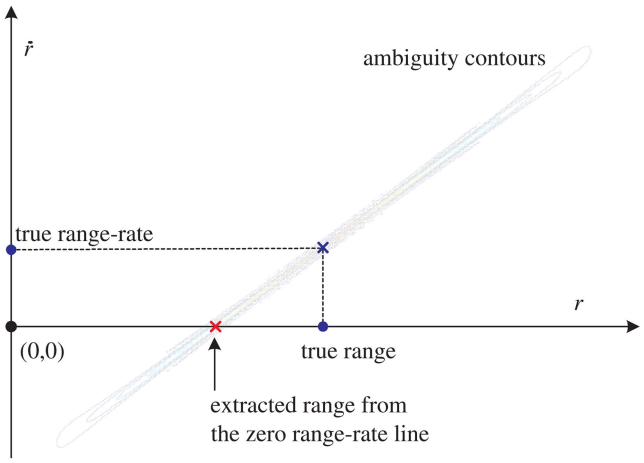

Fig. 1. An illustration of range extraction with a LFM. The target's true position is located at the center of the AF contours in (range, range-rate) plane. The matched filter extracts its range information from zero-range-rate axis; therefore, the measurement will be linearly *biased* by the target range-rate.

In some range-only tracking investigations, the observation is idealized to be true range plus a white Gaussian noise with known distribution. The characteristics of the waveform are neglected. As opposed to the ideal measurement model, the tracking problem is considered from a *system-level* in this paper. The radar system is assumed to utilize a DTW such as LFM to observe a target of interest; as a consequence, the extracted range is actually biased by range-rate (or Doppler). As [2] and [14], the range bias is assumed *linearly* related to the range-rate, with a constant range-Doppler coupling parameter.[1] The uniqueness of DTWs requires a proper mod-

[1]The range bias of a DTW depends on the shape of the decaying ridge of its AF. As for LFM, P3, and P4 waveforms, the ridge is like a tilted line through the zero-delay and zero-Doppler point in the two dimensional AF contour graph [6], and the linear bias modeling in general holds true [2] [14]. A numerical verification of its approximation accuracy can be found in [15].

ification in tracker design; direct application of classic approaches for such biased observations will to some degree degrade tracking performance.

One-dimensional tracking with Doppler biased range measurements has been investigated for a monostatic radar [2], [14]. In [2], Fitzgerald analyzed the measurement accuracy of DTWs, and showed that significant performance loss shall happen if a tracker mistook a biased range observation for an unbiased one. In [14], a steady state α-β filter is formulated for the DTWs, and the stationary estimate covariance is explored against variation of the tracking maneuvering index. In this paper, Doppler biased tracking is extended to distributed configurations including multistatic and multiple-input multiple-output (MIMO) systems. Do the same conclusions hold in the distributed case?

In [2] and [14], the target is assumed to have a constant range-rate; therefore, both the dynamic and measurement equations are linear. For this problem, the Kalman filter is the best, and the tracking potentials of different DTWs could be easily evaluated via a comparison of their stationary estimation results. Unfortunately, the distributed configuration is nonlinear and geometry dependent. No stationary solution is available. Instead of algorithm investigation, we are interested in the performance limitation of DTWs in target tracking, and a Cramér-Rao bound based study is adopted [12], [13]. In this paper, we make the following contributions:

- We model the range-Doppler coupling in two dimensions, and the geometric relationship between the time-varying range and range-rate is derived.
- We give the closed form Posterior Cramér-Rao bounds (PCRB) of Doppler biased tracking for a multistatic configuration.
- We analyze the *tracking* performance of different DTWs respectively with positive, negative, and zero coupling parameters. Numerical results show that the DTW with the positive coupling has lowest bound, while that with a negative one has the highest.
- We investigate the tracking performance of a two-transmitter MIMO radar, of which the waveforms are two DTWs respectively with positive and negative coupling parameters. If the system is power unlimited, a MIMO setup, either co-located or widely-separated, always outperforms the multistatic one. As for the power-limited scenario, the transmitter co-located setup is worse than the multistatic one utilizing DTW with positive coupling parameter, while whether a widely-separated MIMO is better than a multistatic case depends on the geometry.

The present paper collects the multistatic tracking conclusions from [10]; however, significant extensions including the MIMO setups are made. The rest of this paper is as follows: Section 2 introduces the range-Doppler coupling problem; Section 3 gives the tracking model; the PCRB is derived in Section 4; Section 6 analyzes the PCRB of a multistatic radar system, while Section 7 focuses on the performance of the PCRBs for different MIMO configurations; conclusions are drawn after that.

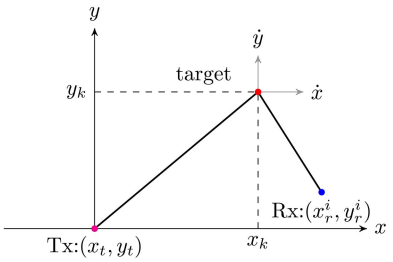

Fig. 2. The bistatic geometry: the coordinates of the transmitter Tx and the ith receiver Rx are respectively located at (x_t, y_t) and (x_r^i, y_r^i), while the target location, $(x_k + \dot{x}t, y_k + \dot{y}t)$, varies linearly with time t due to the constant velocity components projected on either axis.

2. PROBLEM STATEMENT

This paper studies the tracking performance of DTWs, of which the extracted range z of a target of interest is linearly biased by its range-rate $\dot{r}$ [2], [14], [15]

$$z = r + \lambda\dot{r} + n \tag{1}$$

where n denotes additive zero-mean white Gaussian noise, and λ stands for the waveform dependent *range-Doppler coupling parameter*. Generally, λ is known constant for a fixed waveform, and it can be zero, positive, or negative. For example, the coupling parameters of up- and down-sweep LFM waveforms are respectively expressed as $\lambda = f_c\tau/B$ and $\lambda = -f_c\tau/B$ [2], where f_c denotes the carrier frequency, τ is the pulse width, and B stands for the bandwidth.

Firstly, the bistatic range and range-rate are investigated for a given receiver i at the kth pulse repetition period (PRP). Let the coordinates of the transmitter, the ith receiver, and the target initial position at the kth PRP be (x_t, y_t), (x_r^i, y_r^i), and (x_k, y_k), respectively, as in Fig. 2. Then the corresponding bistatic time-varying range $r_k^i(t)$ is

$$\begin{aligned} r_k^i(t) = &\sqrt{(x_k + \dot{x}t - x_r^i)^2 + (y_k + \dot{y}t - y_r^i)^2} \\ &+ \sqrt{(x_k + \dot{x}t - x_t)^2 + (y_k + \dot{y}t - y_t)^2} \end{aligned} \tag{2}$$

where $\dot{x}$ and $\dot{y}$ respectively denotes the target velocity components along x and y axes, and $0 \le t \le \tau$. Suppose that $\dot{x}$ and $\dot{y}$ remain stationary within a single pulse width; the bistatic range-rate $\dot{r}_k^i(t)$ is written as

$$\begin{aligned} \dot{r}_k^i(t) = &\frac{(x_k + \dot{x}t - x_r^i)\dot{x} + (y_k + \dot{y}t - y_r^i)\dot{y}}{\sqrt{(x_k + \dot{x}t - x_r^i)^2 + (y_k + \dot{y}t - y_r^i)^2}} \\ &+ \frac{(x_k + \dot{x}t - x_t)\dot{x} + (y_k + \dot{y}t - y_t)\dot{y}}{\sqrt{(x_k + \dot{x}t - x_t)^2 + (y_k + \dot{y}t - y_t)^2}}. \end{aligned} \tag{3}$$

Obviously, both the bistatic range $r_k^i(t)$ and range-rate $\dot{r}_k^i(t)$ are time-varying. Assume that the target does not

undergo significant spatial shift within a pulse width; thus $r_i(t)$ and $\dot{r}_i(t)$ can be approximated with the individual initial value:

$$\begin{aligned} r_k^i(t) &\approx r_k^i(0) \triangleq r_k^i = d_r^i(x_k, y_k) + d_t(x_k, y_k) \\ \dot{r}_k^i(t) &\approx \dot{r}_k^i(0) \triangleq \dot{r}_k^i = c_x^i(x_k, y_k)\dot{x} + c_y^i(x_k, y_k)\dot{y} \end{aligned} \tag{4}$$

where

$$\begin{aligned} d_r^i(x_k, y_k) &\triangleq \sqrt{(x_k - x_r^i)^2 + (y_k - y_r^i)^2} \\ d_t(x_k, y_k) &\triangleq \sqrt{(x_k - x_t)^2 + (y_k - y_t)^2} \end{aligned} \tag{5}$$

stand for the distances from the target's initial location to the ith receiver and the transmitter, respectively, and

$$\begin{aligned} c_x^i(x_k, y_k) &= \frac{x_k - x_r^i}{d_r^i(x_k, y_k)} + \frac{x_k - x_t}{d_t(x_k, y_k)} \\ c_y^i(x_k, y_k) &= \frac{y_k - y_r^i}{d_r^i(x_k, y_k)} + \frac{y_k - y_t}{d_t(x_k, y_k)}. \end{aligned} \tag{6}$$

Clearly, both r_k^i and $\dot{r}_k^i$ are geometry dependent.

3. TRACKING MODEL

In this section, multistatic tracking is investigated in two dimensions. The coordinates of the target of interest and its corresponding velocity components along the x-axis and y-axis are chosen to compose the state vector

$$\mathbf{s}_k = [x_k, y_k, \dot{x}_k, \dot{y}_k]^T \tag{7}$$

where k indicates the pulse index. A *discrete white noise acceleration model* [1] is employed, of which the dynamic equation is linear

$$\mathbf{s}_{k+1} = \mathbf{F}\mathbf{s}_k + \mathbf{\Gamma}\mathbf{v}_k \tag{8}$$

where

$$\mathbf{F} = \begin{bmatrix} 1 & 0 & T_s & 0 \\ 0 & 1 & 0 & T_s \\ 0 & 0 & 1 & 0 \\ 0 & 0 & 0 & 1 \end{bmatrix} \tag{9}$$

is the time invariant system matrix, T_s denotes the PRP,

$$\mathbf{\Gamma} = \begin{bmatrix} T_s^2/2 & 0 \\ 0 & T_s^2/2 \\ T_s & 0 \\ 0 & T_s \end{bmatrix} \tag{10}$$

denotes the noise gain matrix, and

$$\mathbf{v}_k = [v_x, v_y]^T \tag{11}$$

is the additive process noise vector. In this paper, v_x and v_y are assumed independently and identically distributed (IID) zero-mean white Gaussian noise with variance σ_v^2; as a result, we have $\mathbf{\Gamma}\mathbf{v}_k \sim \mathcal{N}(\mathbf{0}, \mathbf{Q})$, where

$$\mathbf{Q} = \sigma_v^2 \mathbf{\Gamma}\mathbf{\Gamma}^T = \sigma_v^2 \begin{bmatrix} T_s^4/4 & 0 & T_s^3/2 & 0 \\ 0 & T_s^4/4 & 0 & T_s^3/2 \\ T_s^3/2 & 0 & T_s^2 & 0 \\ 0 & T_s^3/2 & 0 & T_s^2 \end{bmatrix} \tag{12}$$

refers to the process noise (target maneuver), which under this model is singular.

Let the multistatic radar system be comprised of a single transmitter and N distributed receivers, all properly synchronized. Each receiver analyzes its individually collected echoes of a certain PRP to estimate the corresponding bistatic range. The range extracted by a matched filter is biased by the bistatic range-rate, and it is written as

$$z_k^i = h_i(\mathbf{s}_k) + w_i \tag{13}$$

for the ith receiver at the kth pulse, where

$$\begin{aligned} h_i(\mathbf{s}_k) = d_r^i(x_k, y_k) + d_t(x_k, y_k) + \lambda c_x^i(x_k, y_k)\dot{x}_k \\ + \lambda c_y^i(x_k, y_k)\dot{y}_k \end{aligned} \tag{14}$$

integrates the range-Doppler coupled bistatic geometry, and w_is stand for the additive IID white Gaussian noise with zero-mean and variance σ_r^2. Defining

$$\begin{aligned} \mathbf{z}_k &= [z_k^1, z_k^2, \ldots, z_k^N]^T \\ \mathbf{h}_k(\mathbf{s}_k) &= [h_1(\mathbf{s}_k), h_2(\mathbf{s}_k), \ldots, h_N(\mathbf{s}_k)]^T \\ \mathbf{w}_k &= [w_1, w_2, \ldots, w_N]^T \end{aligned} \tag{15}$$

the measurement equation is compactly expressed as

$$\mathbf{z}_k = \mathbf{h}_k(\mathbf{s}_k) + \mathbf{w}_k \tag{16}$$

where $\mathbf{w}_k \sim \mathcal{N}(\mathbf{0}, \sigma_r^2 \mathbf{I}_N)$, and $\mathbf{I}_N$ indicates the identity matrix with size $N \times N$.

Compared with an unbiased measurement equation as in [1], (16) contains two Doppler (range-rate) dependent items, $\lambda c_x^i(x_k, y_k)\dot{x}_k$s and $\lambda c_y^i(x_k, y_k)\dot{y}_k$s, to compensate the range bias. This slight modeling modification may significantly improve tracking performance with Doppler biased range measurements [2]. In addition, the measurement model (16) includes the unbiased situation as a special case when $\lambda = 0$.

4. POSTERIOR CRAMÉR-RAO BOUNDS

A. Background

Let $\hat{\boldsymbol{\theta}}$ be the estimate of a random vector $\boldsymbol{\theta}$ based on observation $\boldsymbol{\beta}$. Then the posterior (Bayesian) Cramér-Rao bound (PCRB) for the error covariance matrix satisfies [13]

$$\mathbf{C} \triangleq \mathbb{E}_{\boldsymbol{\theta},\boldsymbol{\beta}}\{(\hat{\boldsymbol{\theta}} - \boldsymbol{\theta})(\hat{\boldsymbol{\theta}} - \boldsymbol{\theta})^T\} \succeq \mathbf{J}^{-1} \tag{17}$$

where $\mathbf{J}$ denotes the Bayesian information matrix (BIM), which is assumed to exist and be invertible, while the matrix inequality indicates that $(\mathbf{C} - \mathbf{J}^{-1})$ is positive

semidefinite. Let

$$\nabla_{\mathbf{a}} = \left[\frac{\partial}{\partial a_1}, \frac{\partial}{\partial a_2}, \ldots, \frac{\partial}{\partial a_n}\right]^T \qquad \text{and} \qquad \Delta_{\mathbf{b}}^{\mathbf{a}} = \nabla_{\mathbf{b}} \nabla_{\mathbf{a}}^T \tag{18}$$

be operators of the first and second-order partial derivatives; hence, $\mathbf{J}$ is written as [13]

$$\mathbf{J} = \mathbb{E}_{\boldsymbol{\theta},\boldsymbol{\beta}}\{-\Delta_{\boldsymbol{\theta}}^{\boldsymbol{\theta}} \ln p(\boldsymbol{\theta},\boldsymbol{\beta})\} \tag{19}$$

where $p(\boldsymbol{\theta},\boldsymbol{\beta})$ denotes the joint probability density function (pdf) of $\boldsymbol{\theta}$ and $\boldsymbol{\beta}$.

For a tracking problem, the parameter vector and observation vector are respectively the collection of states and measurements

$$\boldsymbol{\theta}_k = [\mathbf{s}_1^T, \mathbf{s}_2^T, \ldots, \mathbf{s}_k^T]^T \qquad \text{and} \qquad \boldsymbol{\beta}_k = [\mathbf{z}_1^T, \mathbf{z}_2^T, \ldots, \mathbf{z}_k^T]^T \tag{20}$$

of which the vector sizes depend on the number of pulses. Based on (17), the estimation covariance for $\mathbf{s}_k$ is bounded by the right-lower block of $\mathbf{J}^{-1}$

$$\mathbb{E}_{\boldsymbol{\theta},\boldsymbol{\beta}}\{(\hat{\mathbf{s}}_k - \mathbf{s}_k)(\hat{\mathbf{s}}_k - \mathbf{s}_k)^T\} \succeq [\mathbf{J}^{-1}]_{(4k-3):4k,(4k-3):4k} \tag{21}$$

where $[\mathbf{J}^{-1}]_{(4k-3):4k,(4k-3):4k}$ denotes a submatrix of $\mathbf{J}^{-1}$ spanned with proper elements. Partition $\mathbf{J}$ into blocks

$$\mathbf{J} = \begin{bmatrix} [\mathbf{J}]_{1:4k-1,1:4k-4} & [\mathbf{J}]_{1:4k-4,(4k-3):4k} \\ [\mathbf{J}]_{(4k-3):4k,1:4k-4} & [\mathbf{J}]_{(4k-3):4k,(4k-3):4k} \end{bmatrix} \tag{22}$$

and then we obtain

$$[\mathbf{J}^{-1}]_{(4k-3):4k,(4k-3):4k} = \mathbf{J}_k^{-1}(\lambda) \tag{23}$$

where

$$\begin{aligned} \mathbf{J}_k(\lambda) = {} & [\mathbf{J}]_{(4k-3):4k,(4k-3):4k} - [\mathbf{J}]_{(4k-3):4k,1:4k-4} \\ & \cdot [\mathbf{J}]_{1:4k-1,1:4k-4}^{-1} [\mathbf{J}]_{1:4k-4,(4k-3):4k} \end{aligned} \tag{24}$$

is termed as the *Bayesian information submatrix* (BISM) for the state vector $\mathbf{s}_k$ [12], and λ emphasizes its waveform dependence. With the Markovian assumption

$$p(\boldsymbol{\theta}_k,\boldsymbol{\beta}_k) = p(\boldsymbol{\theta}_{k-1},\boldsymbol{\beta}_{k-1}) p(\mathbf{s}_k \mid \mathbf{s}_{k-1}) p(\mathbf{z}_k \mid \mathbf{s}_k) \tag{25}$$

$\mathbf{J}_k(\lambda)$ can be recursively calculated via the following lemma.

LEMMA 1 *The sequence $\mathbf{J}_k$s of BISMs for the estimate of state vectors $\mathbf{s}_k$s satisfy the recursion*

$$\mathbf{J}_{k+1}(\lambda) = \mathbf{D}_k^{22} - \mathbf{D}_k^{21}(\mathbf{J}_k(\lambda) + \mathbf{D}_k^{11})^{-1}\mathbf{D}_k^{12} \tag{26}$$

where

$$\begin{aligned} \mathbf{D}_k^{11} = {} & \mathbb{E}\{-\Delta_{\mathbf{s}_k}^{\mathbf{s}_k} \ln p(\mathbf{s}_{k+1} \mid \mathbf{s}_k)\} \\ \mathbf{D}_k^{12} = {} & \mathbb{E}\{-\Delta_{\mathbf{s}_k}^{\mathbf{s}_{k+1}} \ln p(\mathbf{s}_{k+1} \mid \mathbf{s}_k)\} = (\mathbf{D}_k^{21})^T \\ \mathbf{D}_k^{22} = {} & \mathbb{E}\{-\Delta_{\mathbf{s}_{k+1}}^{\mathbf{s}_{k+1}} \ln p(\mathbf{s}_{k+1} \mid \mathbf{s}_k)\} \\ & + \mathbb{E}\{-\Delta_{\mathbf{s}_{k+1}}^{\mathbf{s}_{k+1}} \ln p(\mathbf{z}_{k+1} \mid \mathbf{s}_{k+1})\}. \end{aligned} \tag{27}$$

PROOF Proof can be found in [12].

B. PCRB Specification

Based on (8) and (16), $p(\mathbf{s}_{k+1} \mid \mathbf{s}_k)$ and $p(\mathbf{z}_k \mid \mathbf{s}_k)$ are both Gaussian and respectively with conditional pdfs

$$\begin{aligned} p(\mathbf{s}_{k+1} \mid \mathbf{s}_k) = {} & \frac{1}{(2\pi)^2 |\mathbf{Q}|^{1/2}} \\ & \cdot \exp\left[-(1/2)(\mathbf{s}_{k+1} - \mathbf{F}\mathbf{s}_k)^T \mathbf{Q}^{-1} (\mathbf{s}_{k+1} - \mathbf{F}\mathbf{s}_k)\right] \\ p(\mathbf{z}_k \mid \mathbf{s}_k) = {} & \frac{1}{\left(\sqrt{2\pi}\sigma_r\right)^N} \exp\left[-(1/2\sigma_r^2)\|\mathbf{z}_k - \mathbf{h}_k(\mathbf{s}_k)\|^2\right] \end{aligned} \tag{28}$$

where $|\mathbf{Q}|$ denotes the determinant of $\mathbf{Q}$ and $\|\cdot\|$ denotes the l_2 norm. It is easy to verify that

$$\begin{aligned} \mathbf{D}_k^{11} &= \mathbf{F}^T \mathbf{Q}^{-1} \mathbf{F} \\ \mathbf{D}_k^{12} &= -\mathbf{F}^T \mathbf{Q}^{-1} \\ \mathbb{E}\{-\Delta_{\mathbf{s}_{k+1}}^{\mathbf{s}_{k+1}} \ln p(\mathbf{s}_{k+1} \mid \mathbf{s}_k)\} &= \mathbf{Q}^{-1}. \end{aligned} \tag{29}$$

Due to the nonlinearity of $\mathbf{h}_k(\mathbf{s}_k)$, the second term of $\mathbf{D}_k^{22}$ is not straightforward. Fortunately, with the fact that $p(\mathbf{s}_k, \mathbf{z}_k) = p(\mathbf{s}_k) p(\mathbf{z}_k \mid \mathbf{s}_k)$, we have

$$\mathbb{E}\{-\Delta_{\mathbf{s}_k}^{\mathbf{s}_k} \ln p(\mathbf{z}_k \mid \mathbf{s}_k)\} = \mathbb{E}_{\mathbf{s}_k}\{\mathbf{P}_k(\lambda)\} \tag{30}$$

where

$$\mathbf{P}_k(\lambda) \triangleq \mathbb{E}_{\mathbf{z}_k|\mathbf{s}_k}\{-\Delta_{\mathbf{s}_k}^{\mathbf{s}_k} \ln p(\mathbf{z}_k \mid \mathbf{s}_k)\} \tag{31}$$

is a standard Fisher information matrix (FIM) for $\mathbf{z}_k$ [1], [13]. Substituting $p(\mathbf{z}_k \mid \mathbf{s}_k)$ into (31), we have

$$\begin{aligned} \mathbf{P}_k(\lambda) &= \frac{1}{2\sigma_r^2} \sum_{i=1}^N \mathbb{E}_{\mathbf{z}_k|\mathbf{s}_k}\{\Delta_{\mathbf{s}_k}^{\mathbf{s}_k} (z_k^i - h_i(\mathbf{s}_k))^2\} \\ &= \frac{1}{\sigma_r^2} \sum_{i=1}^N \mathbb{E}_{\mathbf{z}_k|\mathbf{s}_k}\{\nabla_{\mathbf{s}_k}[(h_i(\mathbf{s}_k) - z_k^i)\nabla_{\mathbf{s}_k}^T h_i(\mathbf{s}_k)]\} \\ &= \frac{1}{\sigma_r^2} \sum_{i=1}^N \mathbb{E}_{\mathbf{z}_k|\mathbf{s}_k}\{\nabla_{\mathbf{s}_k} h_i(\mathbf{s}_k)\nabla_{\mathbf{s}_k}^T h_i(\mathbf{s}_k)\} \\ &\quad + \frac{1}{\sigma_r^2} \sum_{i=1}^N \Delta_{\mathbf{s}_k}^{\mathbf{s}_k} h_i(\mathbf{s}_k) \mathbb{E}_{\mathbf{z}_k|\mathbf{s}_k}\{h_i(\mathbf{s}_k) - z_k^i\}. \end{aligned} \tag{32}$$

Since $\mathbb{E}_{\mathbf{z}_k|\mathbf{s}_k}\{h_i(\mathbf{s}_k) - z_k^i\} = 0$, $\mathbf{P}_k(\lambda)$ can be simplified as

$$\mathbf{P}_k(\lambda) = \frac{1}{\sigma_r^2} \sum_{i=1}^N \nabla_{\mathbf{s}_k} h_i(\mathbf{s}_k) \nabla_{\mathbf{s}_k}^T h_i(\mathbf{s}_k) \tag{33}$$

where $\nabla_{\mathbf{s}_k} h_i(\mathbf{s}_k)$ is written as

$$\nabla_{\mathbf{s}_k} h_i(\mathbf{s}_k) = \left[\frac{\partial h_i(\mathbf{s}_k)}{\partial x_k}, \frac{\partial h_i(\mathbf{s}_k)}{\partial y_k}, \frac{\partial h_i(\mathbf{s}_k)}{\partial \dot{x}_k}, \frac{\partial h_i(\mathbf{s}_k)}{\partial \dot{y}_k}\right]^T. \tag{34}$$

In the following, the elements of $\nabla_{\mathbf{s}_k} h_i(\mathbf{s}_k)$ will be specified based on (14). Since

$$\begin{aligned}\frac{\partial}{\partial x_k}\{d_r^i(x_k,y_k)+d_t(x_k,y_k)\} &= c_x^i(x_k,y_k)\\ \frac{\partial}{\partial y_k}\{d_r^i(x_k,y_k)+d_t(x_k,y_k)\} &= c_y^i(x_k,y_k)\end{aligned} \tag{35}$$

we have

$$\begin{aligned}\frac{\partial h_i(\mathbf{s}_k)}{\partial \dot{x}_k} &= \lambda c_x^i(x_k,y_k)\\ \frac{\partial h_i(\mathbf{s}_k)}{\partial \dot{y}_k} &= \lambda c_y^i(x_k,y_k)\\ \frac{\partial h_i(\mathbf{s}_k)}{\partial x_k} &= c_x^i(x_k,y_k)+\lambda\dot{x}_k\frac{\partial c_x^i(x_k,y_k)}{\partial x_k}+\lambda\dot{y}_k\frac{\partial c_y^i(x_k,y_k)}{\partial x_k}\\ \frac{\partial h_i(\mathbf{s}_k)}{\partial y_k} &= c_y^i(x_k,y_k)+\lambda\dot{x}_k\frac{\partial c_x^i(x_k,y_k)}{\partial y_k}+\lambda\dot{y}_k\frac{\partial c_y^i(x_k,y_k)}{\partial y_k}\end{aligned} \tag{36}$$

where

$$\frac{\partial c_x^i(x_k,y_k)}{\partial x_k} = \frac{(y_k-y_r^i)^2}{(d_r^i(x_k,y_k))^3}+\frac{(y_k-y_t)^2}{d_t^3(x_k,y_k)} \tag{37}$$

$$\frac{\partial c_y^i(x_k,y_k)}{\partial y_k} = \frac{(x_k-x_r^i)^2}{(d_r^i(x_k,y_k))^3}+\frac{(x_k-x_t)^2}{d_t^3(x_k,y_k)} \tag{38}$$

$$\begin{aligned}\frac{\partial c_x^i(x_k,y_k)}{\partial y_k} &= \frac{\partial c_y^i(x_k,y_k)}{\partial x_k}\\ &= -\frac{(x_k-x_r^i)(y_k-y_r^i)}{(d_r^i(x_k,y_k))^3}-\frac{(x_k-x_t)(y_k-y_t)}{d_t^3(x_k,y_k)}.\end{aligned} \tag{39}$$

Substituting (36) into (33), $\mathbf{P}_k(\lambda)$ can be obtained. Finally, substituting (36) and (29) into (26), the recursion in *Lemma 1* is rewritten as

$$\mathbf{J}_{k+1}(\lambda) = [\mathbf{Q}+\mathbf{F}\mathbf{J}_k^{-1}(\lambda)\mathbf{F}^T]^{-1}+\mathbb{E}_{\mathbf{s}_{k+1}}\{\mathbf{P}_{k+1}(\lambda)\}. \tag{40}$$

The expectation towards $\mathbf{P}_{k+1}(\lambda)$ involves a complicated 4-fold integration. A closed form expression is elusive, hence Monte Carlo methods [3] are usually used.

When $\lambda = 0$, (40) degenerates to the case without range-Doppler coupling. Another special case is the noiseless kinematic model [1], where the state covariance is assumed to be zero, say $\mathbf{Q} = \mathbf{0}$. Hence, the expectation in (40) disappears, and the recursion is simplified to

$$\mathbf{J}_{k+1}(\lambda) = [\mathbf{F}\mathbf{J}_k^{-1}(\lambda)\mathbf{F}^T]^{-1}+\mathbf{P}_{k+1}(\lambda). \tag{41}$$

An implicit assumption behind (40) is that the radar system has perfect detection: the probability of detection is one, while that of false alarm is zero. Such an assumption obviously simplifies PCRB analysis; however, it may not hold true in some practical applications, particularly for those with low signal-to-noise ratio (SNR). An interesting discussion on PCRB with nonideal detection can be found in [8] and [16]; this paper contains no treatment of measurement origin uncertainty.

5. PCRB WITH CONSTANT ACCELERATION

Suppose that the target undergoes a constant acceleration. If its velocity significantly changes within a pulse duration τ, the linear bias model (1) would no longer hold true as the AF will be distorted [5]. In the following, $\ddot{x}\tau$ and $\ddot{y}\tau$ are assumed to be very small (actually, negligible), where $\ddot{x}$ and $\ddot{y}$ respectively denote the acceleration components along x and y axes. This is a fair assumption: for a practical radar pulse duration $\tau = 30\ \mu$s, the velocity change is only 3×10^{-3} m/s even though the acceleration is as high as 100 m/s^2. The time-varying bistatic range for receiver i at the kth pulse is written as

$$\begin{aligned}\bar{r}_k^i(t) = &\sqrt{(x_k+\dot{x}t+0.5\ddot{x}t^2-x_r^i)^2+(y_k+\dot{y}t+0.5\ddot{y}t^2-y_r^i)^2}\\ &+\sqrt{(x_k+\dot{x}t+0.5\ddot{x}t^2-x_t)^2+(y_k+\dot{y}t+0.5\ddot{y}t^2-y_t)^2}\end{aligned} \tag{42}$$

where $0\le t\le\tau$. Since $\ddot{x}t^2 \ll \dot{x}t$ and $\ddot{y}t^2 \ll \dot{y}t$, we have

$$\begin{aligned}\bar{r}_k^i(t) \simeq &\sqrt{(x_k+\dot{x}t-x_r^i)^2+(y_k+\dot{y}t-y_r^i)^2}\\ &+\sqrt{(x_k+\dot{x}t-x_t)^2+(y_k+\dot{y}t-y_t)^2} = r_k^i(t).\end{aligned} \tag{43}$$

Therefore, the geometry results in Section 2 are still applicable for PCRB with a low acceleration.

The PRP is much larger than pulse width. The acceleration effect between pulses cannot be ignored in target tracking. Mathematically, the state vector should be modified as

$$\bar{\mathbf{s}}_k = [x_k, y_k, \dot{x}_k, \dot{y}_k, \ddot{x}_k, \ddot{y}_k]^T. \tag{44}$$

The dynamic equation falls into the *discrete Wiener process acceleration model* [1]

$$\bar{\mathbf{s}}_{k+1} = \bar{\mathbf{F}}\bar{\mathbf{s}}_k+\bar{\mathbf{\Gamma}}\mathbf{v}_k \tag{45}$$

where

$$\bar{\mathbf{F}} = \begin{bmatrix}1&0&T_s&0&T_s^2/2&0\\0&1&0&T_s&0&T_s^2/2\\0&0&1&0&T_s&0\\0&0&0&1&0&T_s\\0&0&0&0&1&0\\0&0&0&0&0&1\end{bmatrix} \tag{46}$$

and

$$\bar{\mathbf{\Gamma}} = \begin{bmatrix}T_s^2/2&0&T_s&0&1&0\\0&T_s^2/2&0&T_s&0&1\end{bmatrix}^T. \tag{47}$$

Based on (43), the contribution of $\ddot{x}$ and $\ddot{y}$ to range is negligible; the measurement equation (14) remains unchanged. Using $\bar{\mathbf{F}}$, $\bar{\mathbf{G}}$, and $\bar{\mathbf{Q}} = \sigma_v^2\bar{\mathbf{\Gamma}}\bar{\mathbf{\Gamma}}^T$ to properly

modify the corresponding parts in Section 4, the PCRB for constant acceleration will be obtained

$$\bar{\mathbf{J}}_{k+1}(\lambda) = [\bar{\mathbf{Q}} + \bar{\mathbf{F}}\bar{\mathbf{J}}_k^{-1}(\lambda)\bar{\mathbf{F}}^T]^{-1} + \mathbb{E}_{\bar{\mathbf{s}}_{k+1}}\{\bar{\mathbf{P}}_{k+1}(\lambda)\} \tag{48}$$

where

$$\begin{aligned}\bar{\mathbf{P}}_k(\lambda) &= \frac{1}{\sigma_r^2}\sum_{i=1}^{N}\nabla_{\bar{\mathbf{s}}_k}h_i(\bar{\mathbf{s}}_k)\nabla_{\bar{\mathbf{s}}_k}^T h_i(\bar{\mathbf{s}}_k)\\ &= \frac{1}{\sigma_r^2}\sum_{i=1}^{N}\nabla_{\bar{\mathbf{s}}_k}h_i(\mathbf{s}_k)\nabla_{\bar{\mathbf{s}}_k}^T h_i(\mathbf{s}_k)\end{aligned} \tag{49}$$

and $\nabla_{\bar{\mathbf{s}}_k}h_i(\mathbf{s}_k)$ is specified as

$$\begin{aligned}\nabla_{\bar{\mathbf{s}}_k}h_i(\mathbf{s}_k) &= \left[\frac{\partial h_i(\mathbf{s}_k)}{\partial x_k}, \frac{\partial h_i(\mathbf{s}_k)}{\partial y_k}, \frac{\partial h_i(\mathbf{s}_k)}{\partial \dot{x}_k}, \frac{\partial h_i(\mathbf{s}_k)}{\partial \dot{y}_k}, 0, 0\right]^T\\ &= [(\nabla_{\mathbf{s}_k}h_i(\mathbf{s}_k))^T, 0, 0]^T.\end{aligned} \tag{50}$$

6. λ: POSITIVE, NEGATIVE OR ZERO?

Were this treated in one dimension (range) the optimal tracker would be Kalman, and the stationary estimation covariance (from the Riccati equation) could reflect the performance of different waveforms. Here, however—in a distributed configuration and working in two Cartesian dimensions—the measurement equations are geometry dependent; no stationary solution exists, hence the performances for different λs are compared with the help of their PCRBs. Let the multistatic radar system be composed by one transmitter and four receivers, of which the coordinates are shown in Fig. 3. The PRP, receiver noise, and maneuvering index [1] are all fixed with values $T_s = 2$ s, $\sigma_r = 5$ m/s and $\kappa = \sigma_v T_s^2/\sigma_r = 1$. The PCRBs of position tracking errors

$$\sqrt{[\mathbf{J}_k^{-1}(\lambda)]_{1,1} + [\mathbf{J}_k^{-1}(\lambda)]_{2,2}} \tag{51}$$

for different λs. Firstly, we compare their tracking performance for a constant velocity target, of which the speed is 400 m/s. The target has four trajectories as shown in Fig. 3, and the calculated results for them are shown in Fig. 4. From those figures, we see that:

- The PCRBs are geometry dependent. The curves with different trajectories have quite dissimilar shapes. In addition, the curves with different λs but the same trajectory have similar shapes, but (slightly) different values.
- The bounds for positive λ are lower than those for a zero λ, while a negative λ introduces a higher bound. However, those of $|\lambda|$ and $-|\lambda|$ are not necessarily symmetric with respect to that of $\lambda = 0$.
- With the increase of λ, the bound becomes lower for a given trajectory. Note that λ is waveform dependent, and $|\lambda|$ cannot be arbitrarily large.

Secondly, the constant acceleration is considered. The target starts from stationary with an acceleration rate

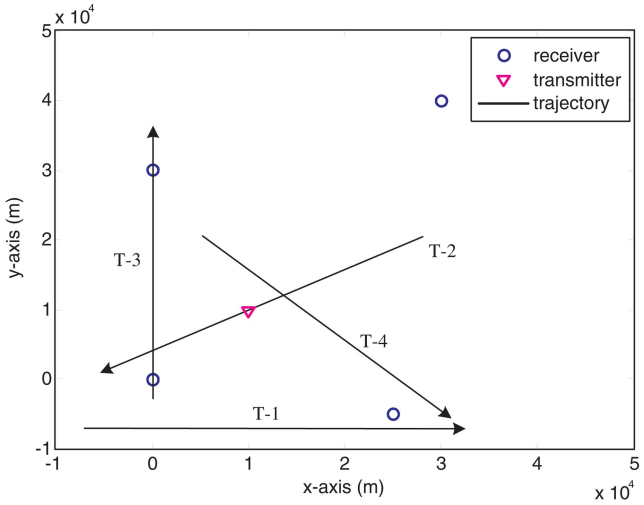

Fig. 3. An illustration of a multistatic constellation with a single transmitter and 4 receivers. Four typical target trajectories are used in the simulation: T-1 stands for a trajectory outside of the constellation, T-2 is the situation crossing the transmitter, T-3 stands for the case crossing the boundary receivers, while T-4 is a general one within the constellation.

15 m/s^2. Its four trajectories share the same initial points and directions as those in the previous example. Their PCRBs are illustrated in Fig. 5. Obviously, similar observations can be found as constant velocity case. Due to their similarity, we will not investigate the acceleration model in the MIMO tracking.

To reemphasize that a positive λ leads to better tracking performance than a negative one is consistent with the theoretical analysis for the monostatic tracking [14]. An intuitive explanation is in Fig. 6. Since the range and range-rate are positively correlated in the state equation, their prior uncertainty can be considered as an ellipse centered at the range and range-rate of truth (the black dot), where the major axis of the ellipse has a positive slope. In the absence of noise, the two measurement extraction lines for waveforms, respectively with slope $\pm\lambda$, traverse the black dot; however, the contamination could slightly shifts them away from the noiseless situations in either direction (dashed lines). The possible shifts engender two measurement uncertainty bands (area between the two parallel dashed lines) as shown in Fig. 6. The uncertainty band for the positive λ and prior uncertainty ellipse share less overlap than that of the negative one. Consequently, a positive λ induces greater error cancelation in updating maintenance and result in better tracking performance.

Interestingly, waveforms with $\pm\lambda$ share the same measurement mean square errors, but with different PCRBs for a distributed configuration. This again verifies that *observations with the same measurement quality do not necessarily result in the same tracking performance* [9]. Moreover, a waveform with positive λ induces a lower bound than that with a zero λ, so the biased measurements are not always bad from the tracking viewpoint if the bias can be properly modeled.

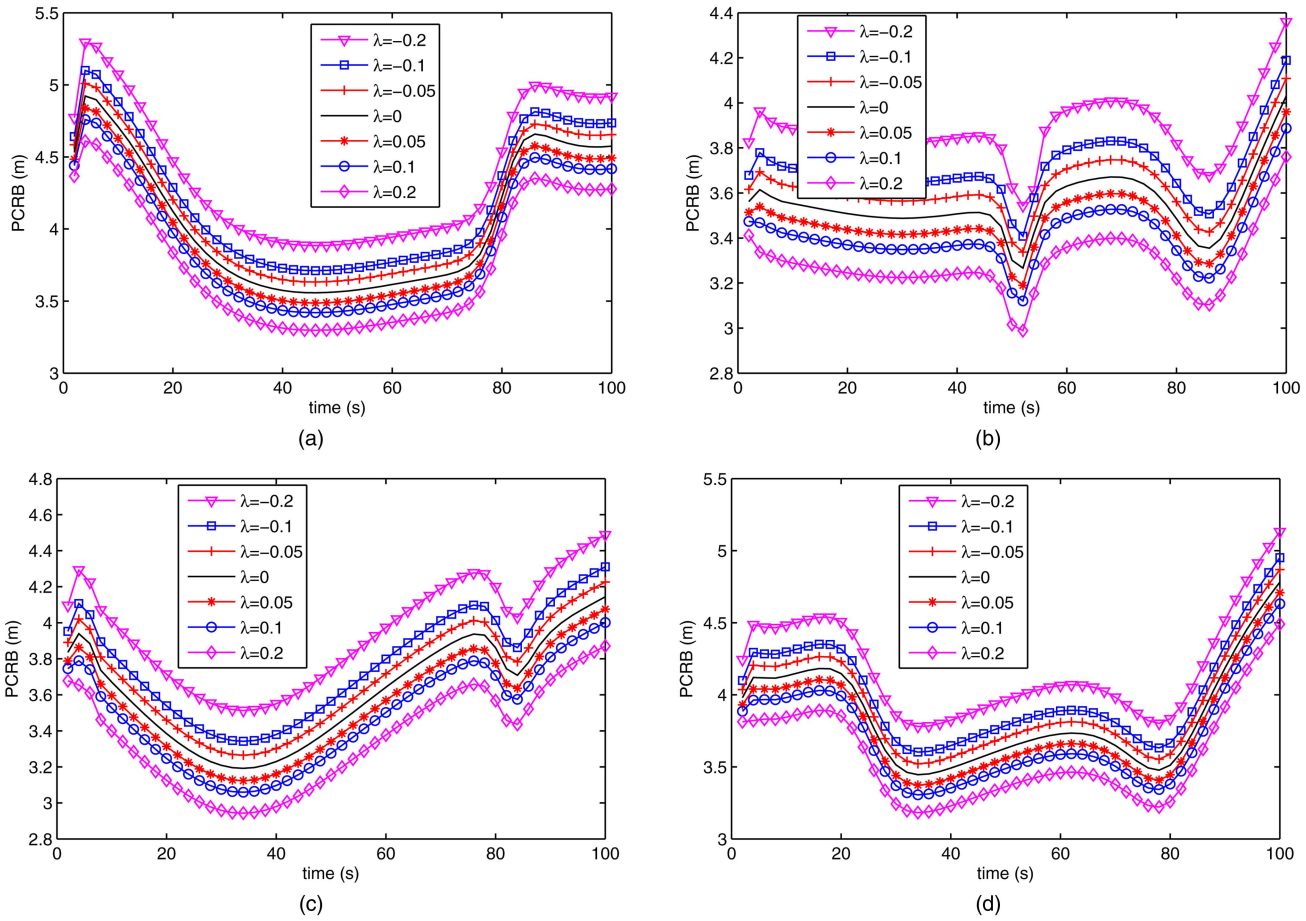

Fig. 4. PCRBs of a multistatic radar with different waveform parameters λs and target trajectories for constant velocity. The multistatic constellation and target trajectories are shown in Fig. 3. The prior distribution is $P_0 = \mathrm{diag}([20,20,5,5])$.

7. MIMO RADAR WAVEFORM COOPERATION

MIMO radar is an emerging concept employing waveform and spatial diversities to improve system performance [4], [7], [11]. Roughly, it can be divided into two categories based on the transmitter configuration: co-located [7] and widely-separated [4]. The multiple transmission trait requires the waveforms to be (nearly) orthogonal. Apparently the up- and down-sweep LFMs have very low cross-correlation even with moderate Doppler shift; therefore, they can be used in a two-transmitter MIMO system [17].

A. Power Unlimited System

Full power transmission is assumed to be performed at each antenna for this scenario. If the transmitters are homogeneous, the total radiated energy doubles as the number of transmitters N_t increases from one to two. Let the waveform energy keep constant; the range variance σ_r^2 remains the same for both multistatic and MIMO radar systems. Suppose the multistatic radar is the special case of the MIMO one via shutting down one transmitter—that is single-input multiple-output (SIMO)—and then we have the following results.

LEMMA 2 *Let $\mathbf{J}_k^{\mathrm{MU}}(\lambda,\sigma_r^2)$ denote the BISM of a power unlimited MIMO radar with two waveforms parameterized with $\pm\lambda$ and noise variance σ_r^2, and let $\mathbf{J}_k^{\mathrm{SU}}(\lambda,\sigma_r^2)$ denote that of a multistatic one with proper parameters. Suppose $\mathbf{J}_k^{\mathrm{MU}}(\lambda,\sigma_r^2) = \mathbf{J}_k^{\mathrm{SU}}(\lambda,\sigma_r^2)$, and then we have $\mathbf{J}_{k+1}^{\mathrm{MU}}(\lambda,\sigma_r^2) \succeq \mathbf{J}_{k+1}^{\mathrm{SU}}(\lambda,\sigma_r^2)$.*

PROOF Proof is straightforward.

In the power unlimited scenario, the MIMO radar is essentially composed of two multistatic ones. Apparently, it can obtain more information about the target, no matter whether the transmitters are co-located or widely-separated.

B. Power Limited System

The total energy is fixed for a power limited system; for simplicity, it is shared uniformly among transmitters. Based on (4) of [14], the measurement variance σ_r^2 is inversely proportional to the waveform power. So it is reasonable to assume that the range variance of the multistatic radar is half of that of a two-transmitter MIMO radar.

1) *Transmitter Co-located Case*: The co-located transmitter configuration does not enhance the spatial diversity. Based on the analysis in the previous section,

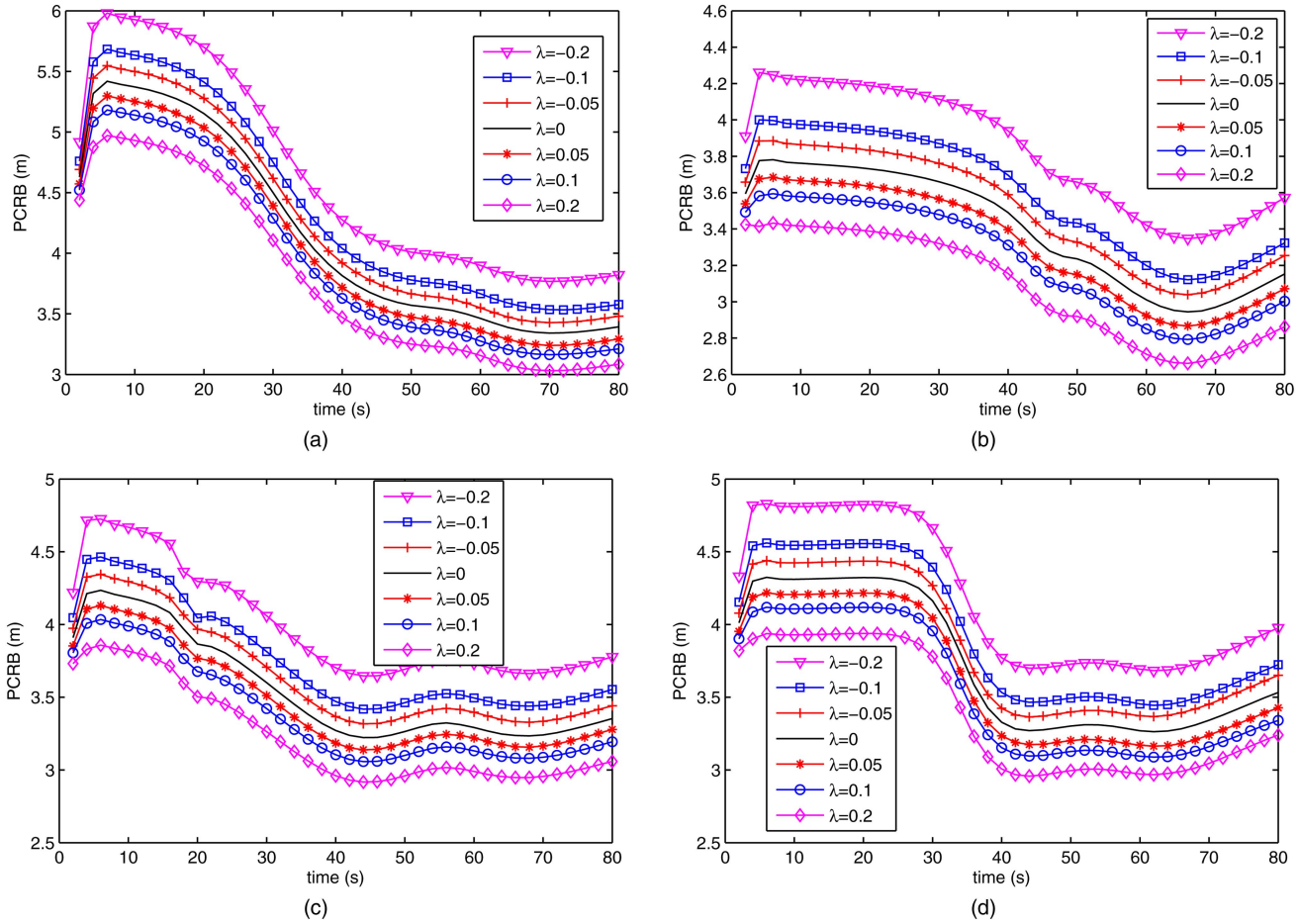

Fig. 5. PCRBs of a multistatic radar with different waveform parameters λs and target trajectories for constant acceleration. The prior distribution is $P_0 = \text{diag}([20,20,5,5,1,1])$.

MIMO is better than the multistatic case with a negative λ, but worse than that with a positive λ. Now, we are still interested in another problem: whether a MIMO radar is better than a multistatic radar with a zero λ. A thorough analysis would be complex; to simplify it, we adopt an assumption that the target is in the far-field of the receivers and transmitters; mathematically, $d_r^i(x_k, y_k)$ and $d_t^i(x_k, y_k)$ are both very large. Since the denominators of each item of $\partial c_x^i/\partial x_k$, $\partial c_y^i/\partial x_y$, and $\partial c_x^i/\partial x_y$ have higher orders than the numerators, we have

$$\frac{\partial c_x^i}{\partial x_k} \approx \frac{\partial c_y^i}{\partial y_k} \approx \frac{\partial c_x^i}{\partial y_k} \approx \frac{\partial c_y^i}{\partial x_k} \approx 0. \tag{52}$$

Moreover, the target speed is assumed low, and $|\lambda|$ is in general small; as a consequence, $\nabla_{\mathbf{s}_k} h_i(k)$ can be approximated as

$$\mathbf{g}_i(\lambda) \triangleq \nabla_{\mathbf{s}_k} h_i(k) \approx [c_x^i, c_y^i, \lambda c_x^i, \lambda c_y^i]^T. \tag{53}$$

Substitute (53) into (33), the FIM is rewritten as

$$\bar{\mathbf{P}}_k(\lambda) = \frac{1}{\sigma_r^2} \sum_{i=1}^{N} \mathbf{g}_i(\lambda)\mathbf{g}_i^T(\lambda) = \frac{1}{\sigma_r^2} \begin{bmatrix} 1 & \lambda \\ \lambda & \lambda^2 \end{bmatrix} \otimes \mathbf{G} \tag{54}$$

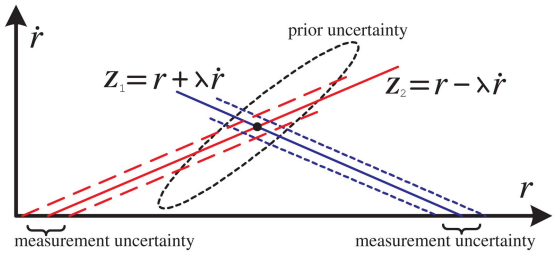

Fig. 6. An intuitive explanation of why a DTW with a positive coupling parameter outperforms that with a negative one in target tracking, where $\lambda > 0$ in this figure. Since the range r and range-rate $\dot{r}$ are positively correlated in the state equation, the prior uncertainty could be considered as an ellipse with positive major axis. If the coupling parameter is positive, the measurement and prior uncertainties will have less overlapping area. Therefore, it has better error cancelation capacity.

where

$$\mathbf{G} = \begin{bmatrix} \sum_{i=1}^{N} (c_x^i)^2 & \sum_{i=1}^{N} c_x^i c_y^i \\ \sum_{i=1}^{N} c_x^i c_y^i & \sum_{i=1}^{N} (c_y^i)^2 \end{bmatrix} \tag{55}$$

is a positive semidefinite matrix.

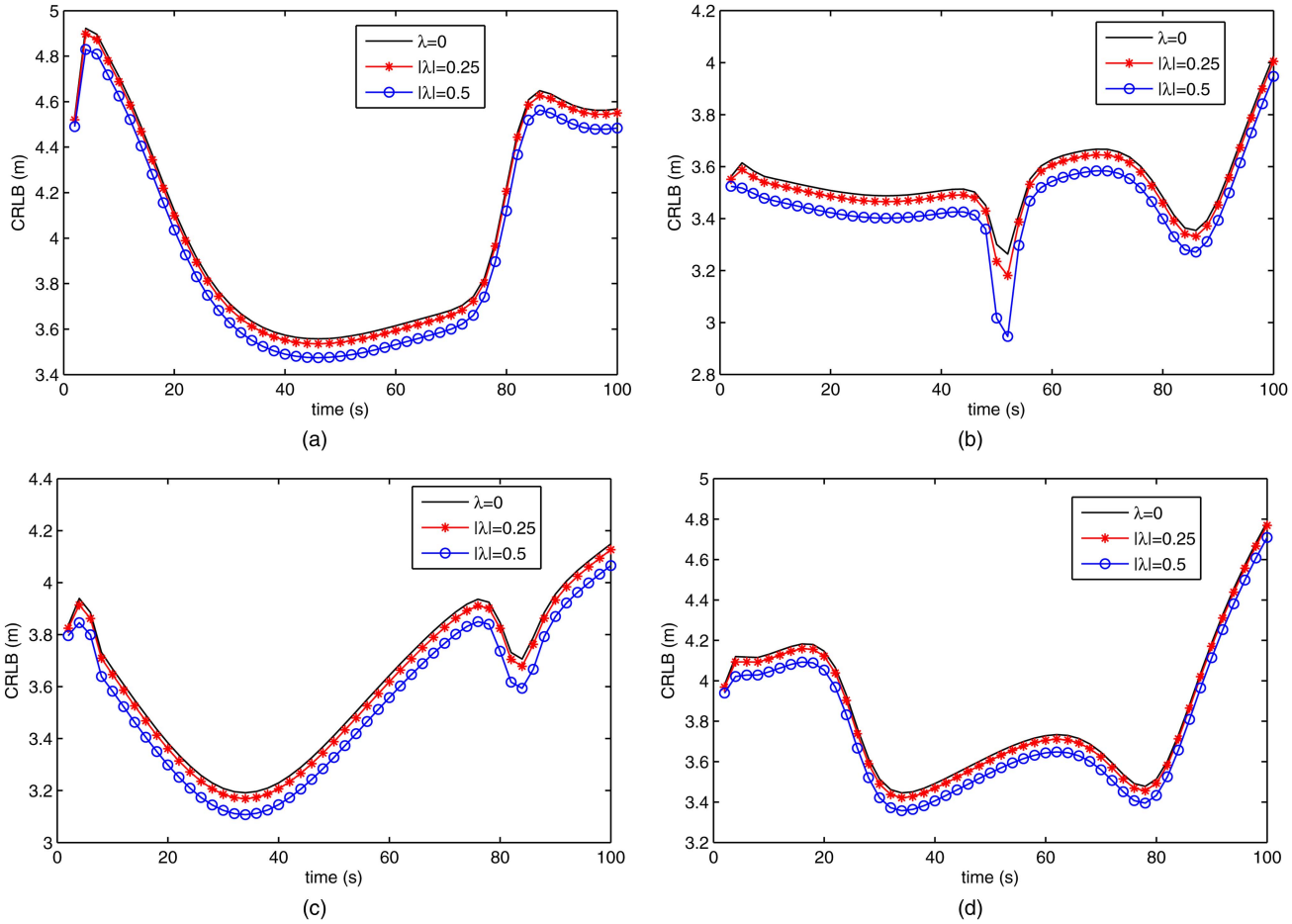

Fig. 7. PCRBs of a transmitter co-located MIMO radar with different waveform parameters λs and target trajectories. The prior distribution is $P_0 = \mathrm{diag}([20, 20, 5, 5])$.

LEMMA 3 *Let* $\mathbf{J}_k^{\mathrm{ML}}(\lambda, 2\sigma_r^2)$ *and* $\mathbf{J}_k^{\mathrm{SU}}(\lambda, \sigma_r^2)$ *respectively denote the BISMs of a power limited co-located MIMO and multistatic radars with proper parameters. Suppose* $\mathbf{J}_k^{\mathrm{ML}}(\lambda, 2\sigma_r^2) = \mathbf{J}_k^{\mathrm{SL}}(0, \sigma_r^2)$ *and (52) holds true, and then we have* $\mathbf{J}_{k+1}^{\mathrm{ML}}(\lambda, 2\sigma_r^2) \succeq \mathbf{J}_{k+1}^{\mathrm{SL}}(0, \sigma_r^2)$.

PROOF If (52) holds true, we have

$$\bar{\mathbf{P}}_{k+1}^{\mathrm{ML}}(\lambda) - \bar{\mathbf{P}}_{k+1}^{\mathrm{SL}}(0) = \frac{2}{\sigma_r^2}\mathrm{Diag}([0, \lambda^2]) \otimes \mathbf{G} \qquad (56)$$

based on (54). Since $\mathrm{Diag}([0, \lambda^2]) \succeq \mathbf{0}$ and $\mathbf{G} \succeq 0$, we have $\mathbb{E}\{\bar{\mathbf{P}}_{k+1}^{\mathrm{ML}}(\lambda)\} \succeq \mathbb{E}\{\bar{\mathbf{P}}_{k+1}^{\mathrm{SL}}(0)\}$. Due to the fact that $\mathbf{J}_k^{\mathrm{ML}}(\lambda, 2\sigma_r^2) = \mathbf{J}_k^{\mathrm{SL}}(0, \sigma_r^2)$, *Lemma 3* can be proven.

To sum up, a co-located MIMO configuration with waveform parameters $\pm\lambda$ can be better than a zero λ multistatic radar, but worse than the multistatic radar with waveform parameter $|\lambda|$ in a power limited scenario. Numerical simulations follow to demonstrate these conclusions. The MIMO radar configuration is the same as the multistatic one in Section 6. The range variance is $2\sigma_r^2$ for the former but σ_r^2 for the latter; the other parameters of MIMO radar keep the same as the multistatic ones. The MIMO PCRBs are in Fig. 7 for different λs and target trajectories. Combining Figs. 4 and 7, it is obvious that the MIMO PCRBs are below that for the multistatic one with $\lambda = 0$, but above those corresponding with parameters $|\lambda|$.

Note that the proof of *Lemma 3* assumes that the trajectory is far away from the antennas; however, the simulation, for example Fig. 7, shows that the conclusion still holds even without the assumption.

2) *Transmitter Widely-separated Case*: If the two transmitters are widely-separated, geometric diversity is improved. The main concern here is whether a MIMO configuration is always better than a multistatic one under a constraint on energy. Based on Section 6, a multistatic radar with positive λ is better than that with negative or zero ones, so the multistatic case with $\lambda \leq 0$ is not considered in comparison.

We inherit the multistatic constellation and trajectories in Fig. 3, and add another transmitter, say T-2, at (20 km, 20 km). The two transmitters evenly share the total energy. Based the previous section, a multistatic radar with a positive λ seems to be best, so we only consider a multistatic radar with a positive λ in this part. The results are in Fig. 8, where 'SIMO-1' and 'SIMO-2' denote the PCRBs for the multistatic radars respectively with T-1 and T-2 as transmitter. 'MIMO-1' represents the scenario with transmitting strategies {T-1,$|\lambda|$} and

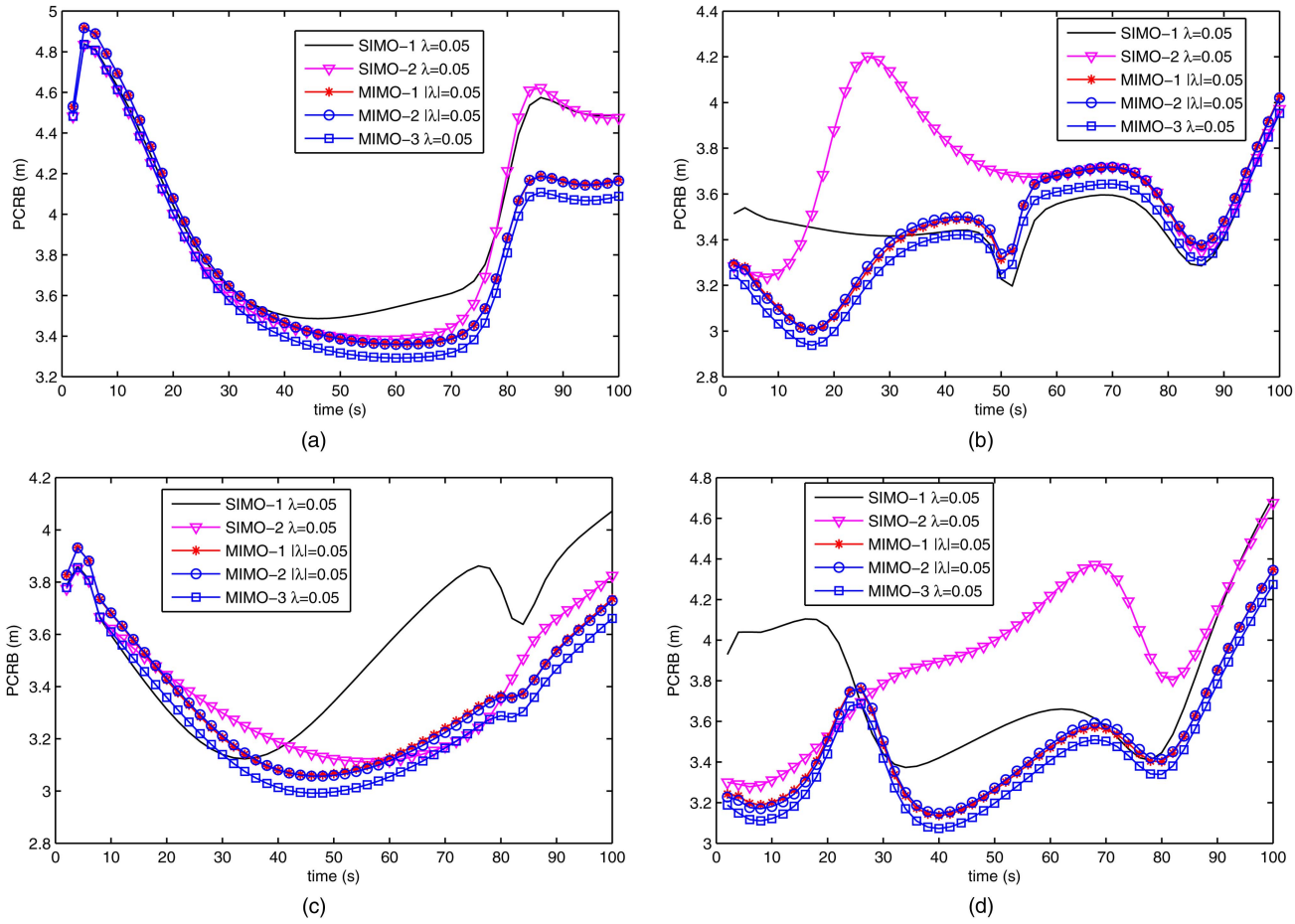

Fig. 8. PCRBs of a transmitter widely-separated MIMO radar with different waveform parameters λs and target trajectories. The prior distribution is $P_0 = \text{diag}([20, 20, 5, 5])$.

{T-2,$-|\lambda|$}, and 'MIMO-2' is for strategies {T-1,-$|\lambda|$} and {T-2,$|\lambda|$}. Finally, 'MIMO-3' stands for the case where both transmitters employ up-sweep LFM; such a system is only possible if the two carrier frequencies are sufficiently separated so as to avoid spectrum interference. From those figures, we observe:

- The PCRBs of 'MIMO-3' are uniformly better than those of 'MIMO-1' and 'MIMO-2' for different trajectories. From a perspective of tracking accuracy, 'MIMO-3' is the best among these three scenarios, even though it has a low spectrum efficiency.
- The PCRBs are highly geometry dependent. As for 'MIMO-3,' 'SIMO-1,' and 'SIMO-2,' no strategy is uniformly better than others.

In short, no uniformly best strategy exists. A clever MIMO radar could adjust transmission scenarios, including waveform assignments and transmitter on-off controlling, to improve its performance.

8. CONCLUSIONS

Range-Doppler coupling is an important characteristic for a Doppler tolerant waveform, where the extracted range is biased by the unknown Doppler shift. The tracking performance of distributed radar systems with range measurements was investigated with the help of the PCRB, and the PCRBs for various parameters and antenna configurations were compared under different energy constraints. The detection processes are assumed ideal, no missed detections nor false alarms. In brief, a waveform with positive range-Doppler coupling (that is, a negative range/range-rate coupling) is a good choice for a multistatic radar or an energy constrained co-located MIMO radar. However, for a transmitter widely-separated configuration, the PCRB is extremely geometry dependent; no uniformly best scenario exists under a power constraint.

REFERENCES

[1] Y. Bar-Shalom, X. R. Li, and T. Kirubarajan
Estimation with Application to Tracking and Navigation.
Wiley-Interscience, 2001.

[2] R. J. Fitzgerald
Effects of range-Doppler coupling on Chirp radar tracking accuracy.
IEEE Transactions on Aerospace and Electronic Systems, **10**, 4 (July 1974), 528–532.

[3] J. E. Gentle
Elements of Computational Statistics.
Springer, 2002.

[4] A. M. Haimovich, R. S. Blum, and L. J. Cimini
MIMO radar with widely separated antennas.
IEEE Signal Processing Magazine, **25**, 1 (Jan. 2008), 116–129.

[5] E. J. Kelly and R. P. Wishner
Matched-filter theory for high-velocity, accelerating targets.
IEEE Transactions on Military Electronics, **9**, 1 (Jan. 1965), 56–69.

[6] N. Levanon and E. Mozeson
Radar Signals.
John Wiley & Sons, Inc., Hoboken, NJ, 2004.

[7] J. Li and P. Stoica
MIMO radar with colocated antennas.
IEEE Signal Processing Magazine, **24**, 5 (Sept. 2007), 106–114.

[8] R. Niu, P. Willett, and Y. Bar-Shalom
Matrix CRLB scaling due to measurements of uncertain origin.
IEEE Transactions on Signal Processing, **49**, 7 (July 2001), 1325–1335.

[9] R. Niu, P. Willett, and Y. Bar-Shalom
Tracking considerations in selection of radar waveform for range and range-rate measurements.
IEEE Transactions on Aerospace and Electronic Systems, **38**, 2 (Apr. 2002), 467–487.

[10] X. Song, P. Willett, and S. Zhou
Posterior Cramér-Rao bounds for Doppler biased multi-static range-only tracking.
In *Proceedings of the International Conference on Information Fusion*, Chicago, IL, July 2011.

[11] X. Song, S. Zhou, and P. Willett
Reducing the waveform cross correlation of MIMO radar with space-time coding.
IEEE Transactions on Signal Processing, **58**, 8 (Aug. 2010), 4213–4224.

[12] P. Tichavsky, C. H. Muravchik, and A. Nehorai
Posterior Cramér-Rao bounds for discrete-time nonlinear filtering.
IEEE Transactions on Signal Processing, **46**, 5 (May 1998), 1386–1396.

[13] H. Van Trees
Detection, Estimation, and Modulation Theory.
John Wiley & Sons, Inc., NY, 1 ed., 1968.

[14] W. Wong and W. D. Blair
Steady-state tracking with LFM waveforms.
IEEE Transactions on Aerospace and Electronic Systems, **36**, 2 (Apr. 2000), 701–709.

[15] X. Zhang, P. Willett, and Y. Bar-Shalom
Tracking considerations in selection of radar waveform given range measurements.
In *Proceedings of 2001 SPIE Annual Conference on Signal and Data Processing of Small Targets*, San Diego, CA, Aug. 2001, vol. 4473, pp. 130–141.

[16] X. Zhang, P. Willett, and Y. Bar-Shalom
Dynamic Cramér-Rao bound for target tracking in clutter.
IEEE Transactions on Aerospace and Electronic Systems, **41**, 4 (Oct. 2005), 1154–1167.

[17] Y. Zhang, G. J. Frazer, and M. G. Amin
Concurrent operation of two over-the-horizon radars.
IEEE Journal of Selected Topics in Signal Processing, **1**, 1 (June 2007), 114–123.

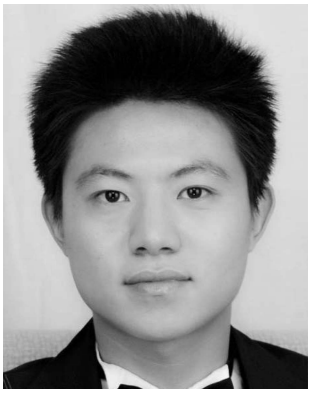

Xiufeng Song (S'08) received the B.S. degree from Xidian University, Xi'an, China, in 2005 and the M.S. degree from Institute of Electronics, Chinese Academy of Sciences (CAS), Beijing, China, in 2008, both in electrical engineering.

He is currently working towards the Ph.D. degree with the Department of Electrical and Computer Engineering, University of Connecticut, Storrs. His research interests lie in signal processing, detection, and estimation theory.

Peter Willett (F'03) received his B.A.Sc. (engineering science) from the University of Toronto in 1982, and his Ph.D. degree from Princeton University in 1986.

He has been a faculty member at the University of Connecticut since 1986, and since 1998 has been a professor. He has published 135 journal articles (13 more under review), 290 conference papers, and 9 book chapters. His primary areas of research have been statistical signal processing, detection, machine learning, data fusion and tracking. He has interests in and has published in the areas of change/abnormality detection, optical pattern recognition, communications and industrial/security condition monitoring.

He is editor-in-chief for *IEEE Transactions on Aerospace and Electronic Systems*, and until recently was associate editor for three active journals—*IEEE Transactions on Aerospace and Electronic Systems* (for Data Fusion and Target Tracking) and *IEEE Transactions on Systems, Man, and Cybernetics*, parts A and B. He is also associate editor for the IEEE AES Magazine, editor of the AES Magazine's periodic Tutorial issues, associate editor for ISIF's electronic *Journal of Advances in Information Fusion*, and is a member of the editorial board of IEEE's Signal Processing Magazine. He was a member of the IEEE AESS Board of Governors 2003–2009. He was general cochair (with Stefano Coraluppi) for the 2006 ISIF/IEEE Fusion Conference in Florence, Italy, Program Co-Chair (with Eugene Santos) for the 2003 IEEE Conference on Systems, Man & Cybernetics in Washington, D.C., and program cochair (with Pramod Varshney) for the 1999 Fusion Conference in Sunnyvale. He was coorganizer of the tracking subsession at the 1999 IEEE Aerospace Conference, and has been organizer of the Remote Sensing Track of that conference 2000–2003. Jointly with T. Kirubarajan he has coorganized the SPIE "System Diagnosis and Prognosis: Security and Condition Monitoring Issues" Conference in Orlando, 2001–2003. He has been a member of the IEEE Signal Processing Society's Sensor-Array & Multichannel (SAM) Technical Committee since 1997, and both serves on that TC's SAM Conferences' Program Committees and maintains the SAM website.

Shengli Zhou (SM'11) received the B.S. degree in 1995 and the M.Sc. degree in 1998, from the University of Science and Technology of China (USTC), Hefei, both in electrical engineering and information science. He received his Ph.D. degree in electrical engineering from the University of Minnesota (UMN), Minneapolis, in 2002.

He has been an assistant professor with the Department of Electrical and Computer Engineering at the University of Connecticut (UCONN), Storrs, 2003–2009, and now is an associate professor. He holds a United Technologies Corporation (UTC) Professorship in Engineering Innovation, 2008–2011. His general research interests lie in the areas of wireless communications and signal processing. His recent focus is on underwater acoustic communications and networking.

Dr. Zhou served as an associate editor for *IEEE Transactions on Wireless Communications*, Feb. 2005–Jan. 2007, and *IEEE Transactions on Signal Processing*, Oct. 2008–Oct. 2010. He is now an associate editor for *IEEE Journal of Oceanic Engineering*. He received the 2007 ONR Young Investigator award and the 2007 Presidential Early Career Award for Scientists and Engineers (PECASE).